Mesoscopic superposition and sub-Planck-scale structure in molecular wave packets

Suranjana Ghosh,[1,*] Aravind Chiruvelli,[2,†] J. Banerji,[1,‡] and P. K. Panigrahi[1,§]
[1]*Physical Research Laboratory, Navrangpura, Ahmedabad-380 009, India*
[2]*University of Massachusetts at Boston, Boston, Massachusetts 02125-3393, USA*
(Received 8 July 2005; published 30 January 2006)

We demonstrate the possibility of realizing sub-Planck-scale structures in the mesoscopic superposition of molecular wave packets involving vibrational levels. The time evolution of the wave packet, taken here as the SU(2) coherent state of the Morse potential describing hydrogen iodide molecules, produces macroscopic-quantum-superposition-like states, responsible for the above phenomenon. We investigate the phase-space dynamics of the coherent state through the Wigner function approach and identify the interference phenomena behind the sub-Planck-scale structures. The optimal parameter ranges are specified for observing these features.

DOI: 10.1103/PhysRevA.73.013411 PACS number(s): 42.50.Md, 03.65.Yz

Mesoscopic superposition of coherent states and their generalizations, such as macroscopic quantum superposition (or catlike) states, have attracted considerable attention in the recent literature [1–3], since they show a host of nonclassical behaviors. In a remarkable paper, Zurek [4] demonstrated that appropriate superposition of some of these states with a classical action A can lead to sub-Planck-scale structures in phase space. These sub-Planck-scale structures in phase space are characterized by an area $\hbar^2/A$. Apart from their counterintuitive nature and theoretical significance, the above scale has been shown to control the effectiveness of decoherence, a subject of tremendous current interest in the area of quantum computation and information. Zurek's realization made use of dynamical systems which exhibit chaotic behavior in the classical domain. Recently a cavity QED realization involving the mesoscopic superposition of the compass states has been given [5]. In principle, one could also use superpositions of catlike states arising in quantum optical systems with large Kerr nonlinearity [2].

In this Rapid Communication, we demonstrate the possibility of realizing sub-Planck-scale structures in the mesoscopic superposition of molecular wave packets, which involves vibrational levels. The time evolution of an initial wave packet, taken here as the SU(2) coherent state (CS) of the Morse potential, produces catlike states. These arise due to the quadratic dependence of the energy on the vibrational quantum number. The superposition of these states is responsible for the above phenomena. We study the spatiotemporal structure of these states, paying special attention to the fractional revival, which gives rise to four coherent states required for the observation of the sub-Planck structure. This structure can be clearly explained through interference phenomena in phase space. For this, we investigate the phase-space dynamics of the coherent state through the Wigner function approach and identify the optimal parameter ranges for a clear observation of these features.

*Electronic address: sanjana@prl.res.in
†Electronic address: Aravind.Chiruvell001@students.umb.edu
‡Electronic address:jay@prl.res.in
§Electronic address: prasanta@prl.res.in

The Morse potential is well known to capture the vibrational dynamics of a number of diatomic molecules [6–10]. It is worth mentioning that the phenomena of revival and fractional revival [11–13] have been experimentally observed in wave packets involving vibrational levels [14]. Creation of the wave packets and observation of their dynamics are carried out through pump-probe method [15]. The control and analysis of molecular dynamics is achieved through ultrashort femtosecond laser pulses [16]. Fractional revival can be probed by random-phase fluorescence interferometry [17]. Recently, catlike states, arising in the temporal evolution of the Morse system, have been proposed for use in quantum logic operations [18].

The Morse potential describing the vibrational motion of a diatomic molecule has the form

$$V(x) = D(e^{-2\beta x} - 2e^{-\beta x}), \tag{1}$$

where $x = r/r_0 - 1$, r_0 is the equilibrium value of the internuclear distance r, D is the dissociation energy, and β is a range parameter. We will be considering the HI molecule, as an example, which has 30 bound states, with $\beta = 2.079\,32$, reduced mass $\mu = 1819.99$ a.u., $r_0 = 3.041\,59$ a.u., and $D = 0.1125$ a.u. Defining

$$\lambda = \sqrt{\frac{2\mu D r_0^2}{\beta^2\hbar^2}}, \quad s = \sqrt{-\frac{8\mu r_0^2}{\beta^2\hbar^2}E}, \tag{2}$$

eigenfunctions of the Morse potential can be written as

$$\psi_n^{\lambda}(\xi) = Ne^{-\xi/2}\xi^{s/2}L_n^s(\xi), \tag{3}$$

where $\xi = 2\lambda e^{-\beta x}$, $0 < \xi < \infty$, and $n = 0, 1, \ldots, [\lambda - 1/2]$, with $[\rho]$ denoting the largest integer smaller than ρ, so that the total number of bound states is $[\lambda - 1/2] + 1$. The parameters λ and s satisfy the constraint condition $s + 2n = 2\lambda - 1$.

Note that λ is potential dependent, s is related to energy E, and, by definition, $\lambda > 0$, $s > 0$. In Eq. (3), $L_n^s(y)$ is the associated Laguerre polynomial and N is the normalization constant:

$$N = \left[\frac{\beta(2\lambda - 2n - 1)\Gamma(n+1)}{\Gamma(2\lambda - n)r_0}\right]^{1/2}. \tag{4}$$

Quite some time back, Nieto and Simmons gave a

minimum-uncertainty coherent state for the Morse oscillator considering suitable conjugate variables [19]. Later, Benedict and Molnár [20] also found the same CS through a supersymmetric quantum-mechanical method. This was used to describe the cat states of the NO molecule [21]. This CS involves an infinite number of bound states, not belonging to the same potential [22]. The Morse potential has a finite number of bound states. Hence it is natural to expect an underlying SU(2) algebra. Recently, Dong *et al.* [23] have obtained the SU(2) generators $\hat{J}_+$, $\hat{J}_-$, and $\hat{J}_0$ which satisfy the algebra at the level of the wave function as

$$[\hat{J}_+,\hat{J}_-]\psi_n^\lambda(\xi) = 2\hat{J}_0\psi_n^\lambda(\xi). \tag{5}$$

The SU(2) Perelomov coherent state of the Morse system is obtained by operating the displacement operator $e^{\alpha\hat{J}_+-\alpha^*\hat{J}_-}$ on the highest bound state n', defined by $\hat{J}_+\psi_{n'}^\lambda(\xi)=0$. Using the disentanglement theorem, the coherent-state modulo normalization becomes

$$\begin{aligned}\chi(\xi) &= e^{-\alpha\hat{J}_-}\psi_{n'}^\lambda(\xi)\\ &= \Bigg[\psi_{n'}^\lambda - \alpha\sqrt{n'(s+n'+1)}\,\psi_{n'-1}^\lambda + \cdots\\ &\quad + \frac{(-\alpha)^{n'}}{(n')!}\sqrt{n'!\,(s+n'+1)(s+n'+2)}\\ &\quad \times \sqrt{\cdots(s+2n')}\,\psi_0^\lambda\Bigg],\end{aligned} \tag{6}$$

As is explicitly seen the above CS involves only the bound states, which are finite in number. This is due to the fact that the underlying group here is a compact group [24]. For the purpose of our analysis, we consider this wave packet. We have checked that superposition of Morse eigenstates with suitable Gaussian weight factors also reproduces the sub-Planck-scale structure.

Simplifying the above expression, we can write it in a compact form

$$\chi(\xi) = \sum_{m=0}^{n'} d_m\psi_m^\lambda(\xi), \tag{7}$$

where

$$d_m = \frac{(-\alpha)^{n'-m}}{(n'-m)!}\left[\frac{n'!\,\Gamma(2\lambda-m)}{m!\,\Gamma(2\lambda-n')}\right]^{1/2}. \tag{8}$$

Figure 1 shows the $|d_m|^2$ distribution of HI molecules for various values of α. For smaller values of α, $|d_m|^2$ is peaked at higher values of m, where the anharmonicity is larger. The corresponding initial CS wave packet is not well localized and has an oscillatory tail. With the increase of α, the $|d_m|^2$ distribution moves towards the lower levels and the wave packet's oscillatory tail gradually disappears. For larger values of α, only the lower levels contribute to form the CS wave packet, where the effect of anharmonicity is rather small. Hence, it is clear that the choice of distribution is quite crucial in the wave packet localization and its subsequent dynamics.

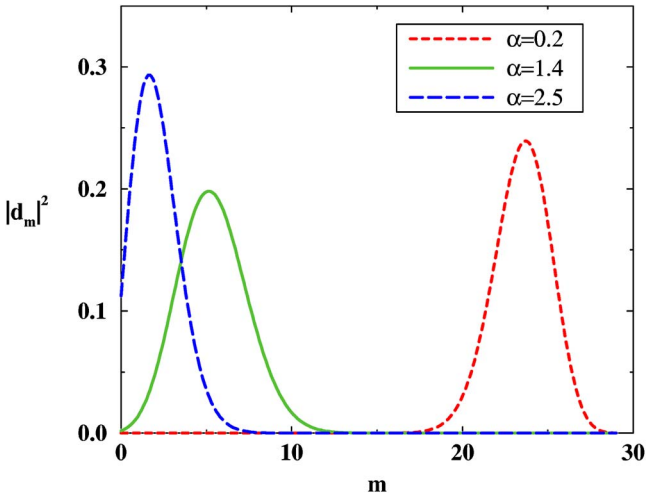

FIG. 1. (Color online) $|d_m|^2$ plotted as a function of m for the Morse potential of the HI molecule for different values of α.

Temporal evolution of the CS state wave packet is given by

$$\chi(\xi,t) = \sum_m d_m\psi_m^\lambda(\xi)\exp[-iE_mt], \tag{9}$$

with $E_m=-(D/\lambda^2)(\lambda-m-1/2)^2$. This quadratic energy spectrum yields classical and revival times given by $T_{\rm cl}=T_{\rm rev}/(2\lambda-1)$ and $T_{\rm rev}=2\pi\lambda^2/D$, respectively. More interestingly, when t takes the values $(r/q)T_{\rm rev}$, where r and q are mutually prime integers, the CS wave packet can be written as a sum of classical CS wave packets [11]:

$$\chi(\xi,t) = \sum_p^{l-1} a_p\chi_{\rm cl}[\xi,(r/qT_{\rm rev}-p/lT_{\rm cl})], \tag{10}$$

where

$$\chi_{\rm cl}(\xi,t) = \sum_m d_m\psi_m^\lambda(\xi)\exp[-2\pi imt/T_{\rm cl}]. \tag{11}$$

The amplitudes are determined by

$$a_p = \frac{1}{l}\sum_m^{l-1}\exp[2\pi i(m^2r/q-mp/l)], \tag{12}$$

where $l=q/2$ when q is an integer multiple of 4 and $l=q$ in all other cases.

Figure 2 shows the CS wave packet in the coordinate representation, where the revival behaviors at $T_{\rm rev}/4$ and $T_{\rm rev}/8$ are not transparent. We will now clarify the phase-space picture of the wave packet at fractional revival times by using the Wigner function approach. We will also show that the interference phenomenon in phase space involving the catlike states gives rise to the sub-Planck-scale structure.

The Wigner function can be written as

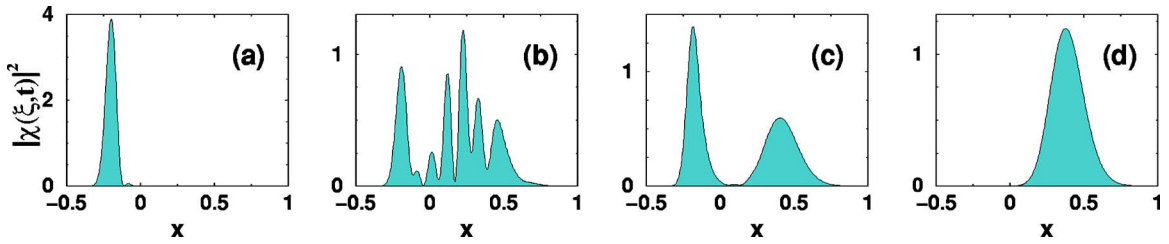

FIG. 2. (Color online) Wave packet distribution in coordinate space for HI molecules, where $\alpha=1.4$, $\beta=2.079\,32$. Plotted here is $|\chi(\xi,t)|^2$ as a function of x (where $\xi=2\lambda\exp[-\beta x]$) for (a) $t=0$, (b) $t=T_{\rm rev}/8$, (c) $t=T_{\rm rev}/4$, and (d) $t=T_{\rm rev}/2$.

$$W(x,p,t)=\frac{r_0}{\pi\hbar}\int_{-\infty}^{+\infty}\bar{\chi}^*(x-x',t)\bar{\chi}(x+x',t)e^{-2ipx'/\hbar}dx', \tag{13}$$

where x is the scaled coordinate and p is the corresponding scaled momentum and also $\bar{\chi}(x)=\chi(\xi)$.

The Wigner functions at instances of fractional revival can be explained by making use of the decomposition of Eq. (10). At $t=T_{\rm rev}/8$, for example, the CS wave packet splits into four classical wave packets:

$$\chi\left(\xi,\frac{T_{\rm rev}}{8}\right)=\frac{1}{2}\left[e^{i\pi/4}\chi_{cl}\left(\xi,\frac{T_{\rm rev}}{8}\right)+\chi_{cl}\left(\xi,\frac{T_{\rm rev}}{8}-\frac{T_{\rm cl}}{4}\right)-e^{i\pi/4}\chi_{cl}\left(\xi,\frac{T_{\rm rev}}{8}-\frac{T_{\rm cl}}{2}\right)+\chi_{cl}\left(\xi,\frac{T_{\rm rev}}{8}-\frac{3T_{\rm cl}}{4}\right)\right]. \tag{14}$$

Defining

$$\chi_{\rm cl}^{\rm (even,odd)}(\xi,t)=\sum_{\rm m_{even,odd}}d_m\psi_m^{\lambda}(\xi)\exp\left[-2\pi i m\frac{t}{T_{\rm cl}}\right], \tag{15}$$

expression (14) can be rewritten in a simpler form

$$\chi\left(\xi,\frac{T_{\rm rev}}{8}\right)=\chi_{\rm cl}^{\rm even}\left(\xi,\frac{T_{\rm rev}}{8}-\frac{T_{\rm cl}}{4}\right)+e^{i\pi/4}\chi_{\rm cl}^{\rm odd}\left(\xi,\frac{T_{\rm rev}}{8}\right). \tag{16}$$

The above expression plays a crucial role in the explanation of the phase-space behavior at $T_{\rm rev}/8$. Substituting this in Eq. (13), the Wigner function at $t=T_{\rm rev}/8$ can be written down as a sum of three terms: $W(x,p,T_{\rm rev}/8)=W^{\rm (even)}+W^{\rm (odd)}+W^{\rm (int)}$, where $W^{\rm (even)}$ and $W^{\rm (odd)}$ are the Wigner functions corresponding to the first and second terms on the right-hand side of Eq. (16) and $W^{\rm (int)}$ is the contribution from the interference between these two terms. In Fig. 3, we have plotted $W(x,p,T_{\rm rev}/8)$ and its constituent parts for two values of α. Note that both $W^{\rm (even)}$ and $W^{\rm (odd)}$ are Wigner functions of catlike states. Each consists of two distinct peaks corresponding to two mesoscopic wave packets and an oscillatory structure at the middle due to quantum interference between them. Furthermore, $W^{\rm (even)}$ is along the east-west direction whereas $W^{\rm (odd)}$is along the north-south. This is because the time arguments of $\chi_{\rm cl}^{\rm even}$ and $\chi_{\rm cl}^{\rm odd}$ differ by $T_{\rm cl}/4$ in Eq. (16). The superposition of the interference regions of $W^{\rm (even)}$ and $W^{\rm (odd)}$ gives rise to the sub-Planck structure in Fig. 3(d). It is worth pointing out that $W^{\rm int}$, as plotted in Fig.

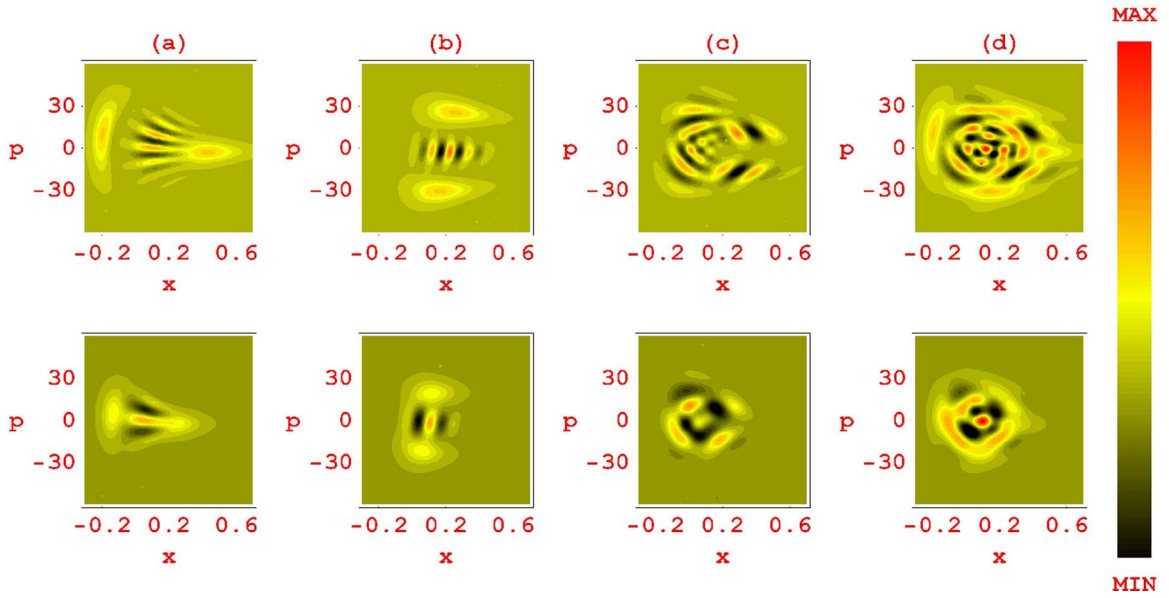

FIG. 3. (Color online) The Wigner function $W(x,p,t)$ and its constituent parts at $t=T_{\rm rev}/8$ as a function of x and p for $\alpha=1.4$ (top row) and $\alpha=2.5$ (bottom row). Shown here are the contour plots of (a)$W^{\rm (even)}$, (b)$W^{\rm (odd)}$, (c)$W^{\rm (int)}$, and (d)$W(x,p,t)$.

3(c), gives the off-diagonal interferences of compasslike states produced at $T_{\mathrm{rev}}/8$.

As seen in Fig. 1, for higher values of α, the initial wave packet involves lower vibrational levels for which the turning points are nearer, resulting in a decrease in the span of the phase space variables. In this case, the area of overlap between the two interference structure increases and the number of ripples become less. As a consequence, the sub-Planck-scale structure at the middle becomes more prominent as shown in the bottom array of Fig. 3. The four mini-wave packets, produced at $T_{\mathrm{rev}}/8$, are not equispaced and not of same size. The asymmetrical nature of the Morse potential is the main reason behind this. We also analyze numerically the expectation values of the position and momentum at $t=T_{\mathrm{rev}}/8$ for different values of α. The uncertainty product $(\Delta x \Delta p)$, obtained from this analysis, is 5.5914 for $\alpha=1.4$ and 2.564 04 for $\alpha=2.5$ in units of $\hbar=1$. The classical action is defined by $A \approx \Delta x \Delta p$ and the corresponding dimension of the sub-Planck-scale structure is $a \approx \hbar^2/A$ [4], which easily comes out to be 0.179 for $\alpha=1.4$ and 0.39 for $\alpha=2.5$, respectively, implying the sub-Planck-scale structure. Note that for smaller values of α the area becomes more sub-Planck.

In conclusion, we have demonstrated that the interesting sub-Planck structure in mesoscopic quantum systems can indeed be realized in the temporal evolution of vibrational wave packets. This is clearly present where four wave packets are produced in the temporal evolution. The coherence parameter α plays a crucial role in the formation of this structure; one needs the low-lying states for a clear observation of this structure. It is worth pointing out that the vibrational wave packets are prone to decoherence through coupling to rotational and other vibrational levels. Recently methods like closed-loop control [25] have been devised to minimize the decoherence effect.

[1] W. Schleich and J. A. Wheeler, Nature (London) **326**, 574 (1987); J. Opt. Soc. Am. B **4**, 1715 (1987); W. Schleich, D. F. Walls, and J. A. Wheeler, Phys. Rev. A **38**, 1177 (1988); W. P. Schleich, *Quantum Optics in Phase Space* (Wiley-VCH, Berlin, 2001) and references therein.

[2] K. Tara, G. S. Agarwal, and S. Chaturvedi, Phys. Rev. A **47**, 5024 (1993).

[3] L. Davidovich, M. Brune, J. M. Raimond, and S. Haroche, Phys. Rev. A **53**, 1295 (1996); J. M. Raimond, M. Brune, and S. Haroche, Phys. Rev. Lett. **79**, 1964 (1997); A. Auffeves *et al.*, *ibid.* **91**, 230405 (2003).

[4] W. H. Zurek, Nature (London) **412**, 712 (2001).

[5] G. S. Agarwal and P. K. Pathak, Phys. Rev. A **70**, 053813 (2004).

[6] P. M. Morse, Phys. Rev. **34**, 57 (1929).

[7] S. I. Vetchinkin, A. S. Vetchinkin, V. V. Eryomin, and I. M. Umanskii, Chem. Phys. Lett. **215**, 11 (1993).

[8] S. I. Vetchinkin and V. V. Eryomin, Chem. Phys. Lett. **222**, 394 (1994).

[9] J. P. Dahl and M. Springborg, J. Chem. Phys. **88**, 4535 (1988).

[10] A. Frank, A. L. Rivera, and K. B. Wolf, Phys. Rev. A **61**, 054102 (2000).

[11] I. Sh. Averbukh and N. F. Perelman, Phys. Lett. A **139**, 449 (1989).

[12] R. Bluhm, V. A. Kostelecky, and J. Porter, Am. J. Phys. **64**, 944 (1996).

[13] R. W. Robinett, Phys. Rep. **392**, 1 (2004) and references therein.

[14] M. J. J. Vrakking, D. M. Villeneuve, and A. Stolow, Phys. Rev. A **54**, R37 (1996).

[15] J. Cao and K. R. Wilson, J. Chem. Phys. **106**, 5062 (1997); A. H. Zewail, J. Phys. Chem. A **104**, 5660 (2000) and references therein.

[16] B. M. Garraway and K. -A. Suominen, Contemp. Phys. **43**, 97 (2002).

[17] Ch. Warmuth *et al.*,J. Chem. Phys. **114**, 9901 (2001).

[18] E. A. Shapiro, M. Spanner, and M. Y. Ivanov, Phys. Rev. Lett. **91**, 237901 (2003).

[19] M. M. Nieto and L. M. Simmons, Jr., Phys. Rev. D **20**, 1321 (1979).

[20] M. G. Benedict and B. Molnár, Phys. Rev. A **60**, R1737 (1999).

[21] P. Földi, A. Czirják, B. Molnár, and M. G. Benedict, Opt. Express **10**, 376 (2002).

[22] T. Shreecharan, P. K. Panigrahi, and J. Banerji, Phys. Rev. A **69**, 012102 (2004).

[23] S. H. Dong, R. Lemus, and A. Frank, Int. J. Quantum Chem. **86**, 433 (2002).

[24] A. M. Perelomov, *Generalized Coherent States and Their Applications* (Springer, Berlin, 1986).

[25] C. Brif, H. Rabitz, S. Wallentowitz, and I. A. Walmsley, Phys. Rev. A **63**, 063404 (2001).